LA-UR-85-0838

Los Alamos National Laboratory is operated by the University of California for the United States Department of Energy under contract W-7405-ENG-36

TITLE: SINGLE KINK DYNAMICS IN AN EASY-PLANE CLASSICAL ANTIFERROMAGNET CHAIN

AUTHOR(S): Gary M. Wysin
Alan R. Bishop
Jaan Oitmaa

SUBMITTED TO: Journal of Physics C.

Los Alamos National Laboratory
Los Alamos, New Mexico 87545

FORM NO 836 R4
ST NO 2629 5/81

SINGLE KINK DYNAMICS IN AN EASY-PLANE CLASSICAL ANTIFERROMAGNET CHAIN

G. M. Wysin[+] and A. R. Bishop
Center for Nonlinear Studies and Theoretical Division
Los Alamos National Laboratory
Los Alamos, NM 87545, U.S.A.

and

J. Oitmaa
School of Physics, The University of New South Wales
P.O. Box 1, Kensington, NSW 2033
AUSTRALIA

J. Phys. C 19, 221 (1986)

[+]Permanent address: LASSP, Cornell University, Ithaca, NY 14853.

Abstract

We present an Ansatz for kink excitations in an easy-plane classical antiferromagnetic chain with a magnetic field in the easy plane. The utility of the Ansatz is that it presents the in-plane (XY) and out-of-plane (YZ) kinks as belonging to one continuously connected energy dispersion curve. Linear stability analysis applied to YZ kinks shows that there is a velocity dependent critical field necessary for stability. We also present results of a numerical integration of the equations of motion which verifies the YZ kink stability regimes, as well as showing that XY kinks are stable over a wide range of fields and velocities.

I. Introduction

Recently there has been considerable experimental and theoretical interest in the low temperature properties of 1-D easy-plane antiferromagnets in the presence of magnetic fields applied in the easy plane. A typical Hamiltonian assumed to describe these materials is (Mikeska 1980):

$$H = \sum_n \{J\vec{S}_n \cdot \vec{S}_{n+1} + A(S_n^z)^2 - g\mu_B B_x S_n^x\} , \qquad (1)$$

where the notation is standard and $J > 0$; $A > 0$ represents the effect of dipole-dipole interactions, and the field B_x is in the easy (XY) plane. Neutron scattering experiments (Heilmann et al. 1979, Boucher et al. 1982) on the $S = 5/2$ compound $(CD_3)_4$ NMn Cl_3 (TMMC), an example of this type of material, have shown an interesting behavior of the in-plane and out-of-plane spin wave dispersions measured as functions of the applied field. In particular, there is evidence for a crossover field, where these spin wave energies become equal, which can be considered to be a switching of the hard anisotropy axis from the dipole anisotropy axis to an axis parallel to the field (Harada et al. 1981).

While this hard axis switching arises simply in a linear spin wave theory, it is also manifested in the nonlinear regime (Harada et al. 1981, Flüggen and Mikeska 1983). The nonlinear dynamics in the continuum limit has been mapped approximately to the sine-Gordon equation, with kink or "soliton" excitations being π rotations of the spins either in the easy plane (XY kinks) or in a plane whose normal is parallel to the field (YZ kinks). These have <u>static</u> energies $g\mu_B B_x S$ and $(8AJS^4)^{\frac{1}{2}}$, so that the critical field at which the two energies are equal is $B_c = (8AJS^2)^{\frac{1}{2}}/(g\mu_B)$. This is the same field for which the in-plane and out-of-plane spin waves (at the zone boundary) have equal energies.

The XY and YZ kinks have previously been considered as distinct special solutions of the continuum equations of motion resulting from (1), belonging to two distinct branches in energy dispersion. Through the application of a variational Ansatz (Wysin 1985), we show here that they are actually just two limits of a single continuously connected dispersion curve. The Ansatz (below) is motivated by a corresponding classical ferromagnet Ansatz used by Liebman et al. (1983). The spins are assumed to rotate in a plane tilted at some angle to the XY plane, with a sine-Gordon motion of the spins in that plane. General features of results derived from this Ansatz are very similar to those for the ferromagnet -- including the existence of a maximum XY kink velocity which is less than the spin wave velocity (see also Wysin et al. 1982, 1984). There is an important difference, however, between the ferromagnetic and antiferromagnetic Ansatz: For the ferromagnet, the ground state is unique, $\vec{S} = (1,0,0)$, while for the antiferromagnet, the ground state is two fold degenerate, with $\vec{S}_{odd} = (\frac{1}{4}\beta, \sqrt{1-\frac{1}{16}\beta^2},0)$, $\vec{S}_{even} = (\frac{1}{4}\beta, -\sqrt{1-\frac{1}{16}\beta^2},0)$ or vice versa, with $\beta \equiv g\mu_B B_x/JS$. In any antiferromagnet Ansatz, the spin at a given lattice site must rotate from one ground state to the other. The fact that the two ground state sublattices are not exactly antiparallel (due to the spin flop effect) leads to considerable complications which cannot be ignored. We should note that for an easy-plane ferromagnet with an Ising symmetry-breaking field ($J < 0$ and $\beta_x S_n^x$ replaced by $\beta_x (S_n^x)^2$ in Eq. (1)) the two degenerate ground states are exactly antiparallel, and this Ansatz precisely reproduces the soliton solutions given by Sklyanin (1979).

We have also considered the stability of kink structures in these systems. This has been approached in two ways: (i) The stability can

be tested by numerical integration of the discrete equations of motion. We have used an initial kink profile obtained from either the XY or YZ sine-Gordon limits of the equations of motion, and followed the time evolution. Alternatively, one can use an initial kink profile as obtained from the Ansatz presented here. Details are given below; or (ii) A linearized stability analysis about sine-Gordon static kink profiles can be used. This can be followed through analytically for the YZ static kinks, but we have not been able to generally solve the stability equations for the XY static kink. We find from both approaches that static YZ kinks are stable only if $B > B_c$; there is no corresponding instability field for static XY kinks -- they are always stable over a wide range of applied field. For moving YZ kinks one finds from the numerical simulations that the stability can either be enhanced or diminished by the motion, depending on whether the motion causes the spins to cant further toward the field or away from it. The linear stability analysis confirms this behavior. The numerical simulations indicate that dynamic XY kinks are always stable.

II. The continuum sine-Gordon limits

First we consider the continuum equations of motion resulting from (1), and the XY and YZ sine-Gordon limits, as given by Flüggen and Mikeska (1983). The spins at the even or odd lattice sites, referred to as the A and B sublattices, have been parametrized in terms of four angles in spherical polar coordinates:

$$\vec{S}_{\substack{A\\B}} = \pm S(\sin(\Theta\pm\theta)\cos(\Phi\pm\phi),\ \sin(\Theta\pm\theta)\sin(\Phi\pm\phi),\ \cos(\Theta\pm\theta)) \ . \qquad (2)$$

S is the length of the spin vectors, and Θ, θ, Φ and ϕ are all functions

of time and position x on the chain. In order to take the continuum limit, we must assume θ, $\phi \ll 1$, as well as slow spatial variations in Φ and Θ. Measuring time in units of $\hbar/JS$, and using the lattice constant as the length unit, the evolution equations are:

$$(\Phi_{xx} - \tfrac{1}{4}\ddot{\Phi})\sin\Theta + 2(\Theta_x\Phi_x - \tfrac{1}{4}\dot{\Theta}\dot{\Phi})\cos\Theta = -\tfrac{1}{4}\beta^2 \sin\Theta \sin\Phi \cos\Phi + \tfrac{1}{2}\beta\dot{\Theta} \sin\Theta \cos\Phi \quad (3a)$$

$$(\Theta_{xx} - \tfrac{1}{4}\ddot{\Theta})\csc\Theta - (\Phi_x^2 - \tfrac{1}{4}\dot{\Phi}^2)\cos\Theta = (\tfrac{1}{4}\beta^2 \cos^2\Phi - \alpha)\cos\Theta - \tfrac{1}{2}\beta\dot{\Phi}\sin\Theta \cos\Phi \ , \quad (3b)$$

where $\beta \equiv g\mu_B B_x/JS$ and $\alpha \equiv 2A/J$, and space and time derivatives are denoted by subscripts and dots, respectively. The "small" angles θ and ϕ are given by:

$$\theta = \tfrac{1}{4}(\beta \cos\Theta \cos\Phi - \dot{\Phi} \sin\Theta) \quad (4a)$$

$$\phi = \tfrac{1}{4} \csc\Theta(\dot{\Theta} - \beta \sin\Phi) \ . \quad (4b)$$

Here we have assumed $\alpha \ll 4$, which is the case for most real materials ($\alpha \cong .04$ for TMMC).

IIA. XY kinks

Statically, Eq. (3b) is satisfied exactly when $\Theta = \tfrac{1}{2}\pi$. Equation (3a) then becomes a static sine-Gordon equation for the variable $\psi \equiv 2\Phi - \pi$. More generally, one can assume $\Theta = \tfrac{1}{2}\pi - \Theta_s$, where $\Theta_s \ll 1$, and linearize the equations in Θ_s: this yields a dynamic sine-Gordon equation for ψ:

$$\psi_{xx} - \tfrac{1}{4}\ddot{\psi} = \tfrac{1}{4}\beta^2 \sin\psi \quad (5a)$$

and

$$(\Theta_{sxx} - \tfrac{1}{4}\ddot{\Theta}_s) + (\Phi_x^2 - \tfrac{1}{4}\dot{\Phi}^2 + \tfrac{1}{4}\beta^2\cos^2\Phi - \alpha)\Theta_s = \tfrac{1}{2}\beta\dot{\Phi} \cos\Phi \ . \quad (5b)$$

A kink solution to Eqs. (5), for $\beta^2 << \alpha$, is a π rotation in the XY plane, moving as a traveling-wave at velocity v:

$$\phi = \frac{\pi}{2} + 2 \tan^{-1} \exp(\tilde{z}); \quad \tilde{z} \equiv \tfrac{1}{2}\beta\gamma(x-vt) \tag{6a}$$

$$\theta_s = -\tfrac{1}{4}(\beta^2\gamma v/\alpha) \operatorname{sech}^2(\tilde{z}); \quad \gamma \equiv (1-\tfrac{1}{4}v^2)^{-\frac{1}{2}} . \tag{6b}$$

Note that the spin wave velocity c = 2 in these units. Although solution (6) is valid only at low fields, we have used these profiles as initial conditions in numerical simulations for arbitrary β. The energy of the kink in Eq. (6) is $E_{XY} = \beta\gamma JS^2$ plus corrections which depend on β^2/α. There is considerable experimental evidence in TMMC demonstrating the existence of these modes (Boucher and Renard 1980, Boucher et al. 1983, 1984, Regnault et al. 1982).

II.B. YZ kinks

Equation (3a) is satisfied exactly by taking $\phi = \frac{1}{2}\pi$, in which case (3b) becomes a sine-Gordon equation in the variable $2\theta - \pi$. The dynamic kink solution is now a π rotation in the YZ plane:

$$\theta = \frac{\pi}{2} + 2 \tan^{-1} \exp(z) \; ; \; z \equiv \gamma\sqrt{\alpha}(x-vt) . \tag{7}$$

Although result (7) has been obtained "exactly" within the small angle approximations $\theta, \phi << 1$, substituting (7) into (4) one finds $\theta = 0$, but

$$\phi = \tfrac{1}{4}(\gamma\sqrt{\alpha}v \operatorname{sech}z+\beta)\coth z . \tag{8}$$

Thus at the center of the kink (z=0), ϕ is no longer small as has been assumed, and this solution is not valid. The profile has an unphysical cusp in S^x which prohibits its use as initial conditions in numerical simulations.

One can correct this problem, and still obtain an exact sine-Gordon equation for YZ kinks, by using a more appropriate coordinate system. Spherical polar coordinates, where the x-axis (i.e., the field direction) is the polar axis, exploit the symmetry of the YZ kinks. With this motivation, we have re-parametrized the spins in terms of new angles θ, θ, Φ, ϕ in x-polar spherical coordinates:

$$\vec{S}_{\substack{A\\B}} = \pm S(\cos(\Theta\pm\theta),\ \sin(\Theta\pm\theta)\cos(\Phi\pm\phi),\ \sin(\Theta\pm\theta)\sin(\Phi\pm\phi)) \ . \qquad (9)$$

The dynamical equations for the four variables now become (Wysin 1985)

$$\begin{aligned}
\dot{\theta} &= 4\phi\sin\theta + \alpha(\phi\sin\theta\cos 2\Phi + \tfrac{1}{2}\theta\cos\theta\sin 2\Phi) \\
\dot{\phi} &= -4\theta\csc\theta + \alpha(\theta\sin\theta\sin^2\Phi - \phi\cos\theta\sin 2\Phi) - \beta \\
\dot{\theta} &= -(2\Phi_x\theta_x + 4\phi\theta)\cos\theta - \Phi_{xx}\sin\theta + \tfrac{1}{2}\alpha\sin\theta\sin 2\Phi \\
\dot{\phi} &= -(4\phi^2 + \Phi_x^2 - 4\theta^2\csc^2\theta)\cos\theta + \theta_{xx}\csc\theta - \alpha\cos\theta\sin^2\Phi \ .
\end{aligned} \qquad (11)$$

Elimination of the small angles θ, $\phi \ll 1$, under the assumption $\alpha \ll 4$, leads to equations similar in structure to Eqs. (3) and (4):

$$(\Phi_{xx} - \tfrac{1}{4}\ddot{\Phi})\sin\theta + 2(\theta_x\Phi_x - \tfrac{1}{4}\dot{\theta}\dot{\Phi})\cos\theta = \tfrac{1}{2}\alpha\sin\theta\sin 2\Phi + \tfrac{1}{2}\beta\dot{\theta}\cos\theta \qquad (12a)$$

$$(\theta_{xx} - \tfrac{1}{4}\ddot{\theta})\csc\theta - (\Phi_x^2 - \tfrac{1}{4}\dot{\Phi}^2)\cos\theta = (\alpha\sin^2\Phi - \tfrac{1}{2}\beta^2)\cos\theta - \tfrac{1}{2}\beta\dot{\Phi}\cos\theta \qquad (12b)$$

$$\phi = \tfrac{1}{4}\dot{\theta}\csc\theta \qquad (13a)$$

$$\theta = -\tfrac{1}{4}(\beta + \dot{\Phi})\sin\theta \ . \qquad (13b)$$

The YZ kink is now found by taking $\theta = \frac{1}{2}\pi$, which satisfies (12b) exactly, and then (12a) becomes a sine-Gordon equation for 2Φ, with kink solution

$$\Phi = 2\tan^{-1} \exp z; \quad \phi = 0 \tag{14a}$$

$$\theta = -\tfrac{1}{4}(\beta - \gamma\sqrt{\alpha}v \operatorname{sech} z) \ . \tag{14b}$$

We now have smooth functions for θ and ϕ, and we have used this profile as initial conditions for numerical simulations. The kink in Eq. (14) has energy

$$E_{YZ} = 2\gamma\sqrt{\alpha}\left(1-\frac{\beta^2}{32}(1-\tfrac{1}{4}v^2)\right).$$

IIC. YZ stability analysis

The stability of the YZ kink solution to Eq. (12) can be determined by assuming small perturbations $\tilde{\Theta}$, $\tilde{\theta}$, $\tilde{\Phi}$, $\tilde{\phi}$ about the sine-Gordon solution Θ_o, θ_o, Φ_o, ϕ_o, substituting into (11) and linearizing in these perturbations. The small angles $\tilde{\theta}$, $\tilde{\phi}$ can be eliminated from the resulting equations, and we obtain decoupled equations for $\tilde{\Theta}$, $\tilde{\Phi}$. For $\alpha << 4$, they are

$$\tilde{\Theta}_{xx} + (\phi_{ox}^2 - 4\theta_o^2 + \alpha\sin^2\Phi_o)\tilde{\Theta} = \tfrac{1}{4}\ddot{\tilde{\Theta}} \tag{15a}$$

$$\tilde{\Phi}_{xx} - \alpha \cos 2\Phi_o \, \tilde{\Phi} = \tfrac{1}{4}\ddot{\tilde{\Phi}} \ . \tag{15b}$$

We assume $\tilde{\Theta} \sim e^{i\omega_1 t}$, $\tilde{\Phi} \sim e^{i\omega_2 t}$ time dependences, and using Eqs. (14), (15) yields the eigenvalue problems (Wysin 1985)

$$-\gamma^2\tilde{\theta}_{zz} + (1-2\ \mathrm{sech}^2\ z - \frac{\beta\gamma v}{2\sqrt{\alpha}}\ \mathrm{sech}\ z)\tilde{\theta} = \lambda_1\ \tilde{\theta} \tag{16a}$$

$$-\gamma^2\ \tilde{\Phi}_{zz} + (1-2\ \mathrm{sech}^2\ z)\tilde{\Phi} = \lambda_2\tilde{\Phi} \tag{16b}$$

with

$$\omega_1^2 = 4\alpha(\lambda_1-1)+ \beta^2 \tag{16c}$$

$$\omega_2^2 = 4\alpha\lambda_2 \tag{16d}$$

For a zero velocity kink, both equations have sech(z) bound state solutions, with eigenvalues $\lambda_1 = \lambda_2 = 0$. The corresponding eigenfrequencies are

$$\begin{aligned} \omega_1^2 &= \beta^2 - 4\alpha \\ \omega_2^2 &= 0\ . \end{aligned} \tag{17}$$

The bound state associated with the $\tilde{\Phi}$ variable is the Goldstone translation mode and involves no structural instability. The bound state for $\tilde{\theta}$, however, can have an imaginary eigenfrequency indicating an instability.[++] Specifically, for fields $\beta^2 < 4\alpha$, static YZ kinks are unstable, and the mode responsible for this instability causes the spins to tilt away from the z-axis. This result has been confirmed by numerical integration of the discrete equations of motion. Starting from a static YZ kink profile, the spins move toward a configuration involving a lower energy XY kink, with the excess energy given to spin waves. Conversely, for $\beta^2 > 4\alpha$, static YZ kinks have been found numerically to be stable.

[++]The analysis by Flüggen and Mikska (1983) did not reveal this instability due to their use of z-polar spherical coordinates.

For nonzero v, the potential for $\tilde{\theta}$ is modified, and therefore so is the bound state eigenvalue λ_1. If v is positive, then the potential becomes deeper, and therefore λ_1 becomes less than zero. From (16c), the field necessary for the kink to be stable is now $\beta^2 > 4\alpha(1-\lambda_1)$; that is, a kink with positive velocity requires a larger field to be stable than does the static kink. For a kink with negative velocity, the opposite is true -- a smaller field is necessary. Even if $\beta^2 < 4\alpha$, there can be stable moving YZ kinks. This has been verified by numerical simulation.

These comments can be made quantitative by estimating $\lambda_1(v)$ using perturbation theory. A simple first order calculation gives $\lambda_1(v) \cong -(\pi\beta/4\alpha^{\frac{1}{2}})(v/c)$; to get a result correct to order $(v/c)^2$ one needs to use second order perturbation theory (Wysin 1985). To first order in v/c, then, the stability criterion $\omega_1^2 > 0$ for moving YZ kinks becomes $v/c < (\beta^2-4\alpha)/(\pi\beta\alpha^{\frac{1}{2}})$. The numerical simulation (section IV) gives results consistent with this relationship.

It should be noted that this direction dependent stability does not really imply a preferred direction of motion for YZ solitons, since we have presented the stability arguments only for one of the four possible soliton solutions (there are two kinks and two antikinks possible). The conclusion that can be drawn, however, is that those YZ solitons in which the motion causes the spins to cant further toward the field (compared to the ground state canting) have increased stability.

III. The Variational Ansatz

In the above discussion the XY and YZ kinks have been assumed to be two independent types of excitations. For a dynamic XY kink, the spins of the A sublattice rotate approximately in a plane tilted at an

angle θ_A to the XY plane, while the spins of the B sublattice move in a similar plane which may be at a slightly different angle θ_B. For low velocity kinks θ_A and θ_B are near zero, and as the velocity increases so do θ_A and θ_B. For dynamic YZ kinks, θ_A and θ_B are near $\frac{1}{2}\pi$, and should approximately satisfy $\theta_A = \frac{1}{2}\pi - \delta$, $\theta_B = \frac{1}{2}\pi + \delta$, where δ is a small parameter. (In fact, the Ansatz predicts that δ is proportional to the velocity.) These observations suggest that one can make an Ansatz for a general kink excitation which will include both the XY and YZ kinks as special limiting cases. The Ansatz will involve variational parameters θ_A, θ_B and a width w, these parameters being determined by extremizing the Lagrangian with respect to the parameters. This Ansatz calculation closely parallels a similar one for the corresponding ferromagnet (Liebmann et al 1983).

An appropriate Ansatz for the xyz components of unit length spins, $\hat{\sigma}_A$, $\hat{\sigma}_B$, is constructed as follows: Consider the spins on the A sublattice first. The trajectory on the unit sphere must be an arc starting from one ground state $(\frac{1}{4}\beta, -(1-\beta^2/16)^{\frac{1}{2}}, 0)$, passing through a point (cos q, 0, sin q) at the center of the kink, and then ending at the opposite ground state $(\frac{1}{4}\beta, +(1-\beta^2/16)^{\frac{1}{2}}, 0)$. The plane in which the tips of the spin vectors move is tilted on an angle θ_A, such that $\tan\theta_A = \sin q/(\cos q - \frac{1}{4}\beta)$ (see Fig. 1). In the $x'y'z'$ coordinate system, obtained by rotating the xyz system through θ_A about the y axis, the equation of this plane is simply $z' = -\frac{1}{4}\beta \sin\theta_A$. In order to determine the x' and y' components of this trajectory, consider the sum and difference vectors $\vec{M} = \frac{1}{2}(\hat{\sigma}_A + \hat{\sigma}_B)$, $\vec{N} = \frac{1}{2}(\hat{\sigma}_A - \hat{\sigma}_B)$ (supposing for the moment that the B sublattice moves in the same plane). The vector $\vec{M}$ approximately traces out a circle of radius $r_M = \frac{1}{8}\beta\cos\theta_A$, with center at

$(x',y') = (\frac{1}{8}\beta\cos\theta_A, 0)$. The vector $\vec{N}$ approximately traces out a semicircle of radius $r_N = (1-\beta^2/16)^{\frac{1}{2}}$, centered at $(x',y') = (0,0)$. Therefore we take (see Fig. 2)

$$M_{x'} = r_M(1+\cos\phi_{sG}) = 2r_M \tanh^2 z \tag{18a}$$

$$M_{y'} = r_M \sin\phi_{sG} = -2r_M \tanh z \operatorname{sech} z \tag{18b}$$

$$N_{x'} = r_N \sin(\tfrac{1}{2}\phi_{sG}) = r_N \operatorname{sech} z \tag{18c}$$

$$N_{y'} = -r_N \cos(\tfrac{1}{2}\phi_{sG}) = r_N \tanh z \tag{18d}$$

where

$$\phi_{sG} = 4\tan^{-1}\exp(z)\ ;\ z = \frac{x-vt}{w}\ . \tag{19}$$

Transforming back to the $\hat{\sigma}$ variables, it is necessary to multiply the $x'y'$ components by a factor $f_A(z) = (1-\sin^2\varepsilon_A \operatorname{sech}^2 z)^{-\frac{1}{2}}$, in order to keep the spin length fixed (ε_A is shown in Fig. 1). If we assume now that the A and B sublattices rotate in planes at different angles θ_A and θ_B, then we can write the Ansatz as follows:

$$\sigma_{Ax'} = f_A(z)\ (M_{x'}+N_{x'})\ ,\ \sigma_{Bx''} = f_B(z)\ (M_{x''}-N_{x''})\ ,$$

$$\sigma_{Ay'} = f_A(z)\ (M_{y'}+N_{y'})\ ,\ \sigma_{By''} = f_B(z)\ (M_{y''}-N_{y''})\ , \tag{20}$$

$$\sigma_{Az'} = -\tfrac{1}{2}\beta\sin\theta_A\ ,\ \sigma_{Bz''} = -\tfrac{1}{2}\beta\sin\theta_B\ .$$

Here single primes refer to the "A" coordinate system at angle θ_A, while double primes refer to the "B" coordinate system at angle θ_B. The single function ϕ_{sG} describes the distribution of the spins on the trajectories for both sublattices.

Using energy units JS^2, and time units $\hbar/JS$, the continuum limit Lagrangian is:

$$L = \int dx\{\tfrac{1}{2} \sum_{i=A,B} [\sigma_i^z \frac{d}{dt} \tan^{-1} (\frac{\sigma_i^y}{\sigma_i^x}) - \tfrac{1}{2} \alpha(\sigma_i^z)^2 + \tfrac{1}{2}\beta\sigma_i^x]$$

$$- (\hat{\sigma}_A \cdot \hat{\sigma}_B - \tfrac{1}{2} \frac{d\hat{\sigma}_A}{dx} \cdot \frac{d\hat{\sigma}_B}{dx})\} \ . \qquad (21)$$

The first term in Eq. (21) is simplified by changing $\sigma_A^z \to \sigma_A^z - 1$ and $\sigma_B^z \to \sigma_B^z + 1$, which changes the Lagrangian by an additive constant that depends only on β, and removes unphysical step functions at $\theta_A = \frac{1}{2}\pi$ and $\theta_B = -\frac{1}{2}\pi$. Since we minimize L with respect to the variational parameters w, θ_A and θ_B, this constant does not affect any of the results that follow. After rotating the Ansatz back to the original xyz coordinate system, and considering $\sqrt{\alpha}$, β and $\Delta \equiv \theta_B - \theta_A$ as small parameters, the Lagrangian (relative to the ground state) is found to be (Wysin 1985):

$$L(\theta_A,\Delta,w) = vK(\theta_A,\Delta) - \frac{1}{w} F(\theta_A,\Delta) - wG(\theta_A,\Delta) \ , \qquad (22a)$$

where

$$F(\theta_A,\Delta) = (r_N^2 - \frac{\beta^2}{48} \cos^2\theta_A) - (\frac{\pi\beta}{16} r_N \sin\theta_A)\Delta - \frac{1}{6} \Delta^2 \qquad (22b)$$

$$G(\theta_A,\Delta) = (\alpha r_N^2 \sin^2\theta_A + \tfrac{1}{4} \beta^2 \cos^2\theta_A) + \tfrac{1}{2}(\alpha r_N^2 - \tfrac{1}{4} \beta^2)\sin 2\theta_A \cdot \Delta + \Delta^2 \qquad (22c)$$

$$K(\theta_A,\Delta) = \pi + \Delta + \frac{\pi\beta}{4} (\sin\theta_A + \tfrac{1}{2}\Delta\cos\theta_A) \equiv k_o + k_1\Delta \ . \qquad (22d)$$

Minimization of L with respect to the width w leads to

$$L = vK - E \tag{23a}$$

$$E(\theta_A,\Delta) = 2[F(\theta_A,\Delta)G(\theta_A,\Delta)]^{\frac{1}{2}} \cong e_o + e_1\Delta + \tfrac{1}{2}e_2\Delta^2 \ , \tag{23b}$$

where e_o, e_1, e_2 are functions of θ_A. Next, if we minimize with respect to Δ, we obtain

$$\Delta = (vk_1 - e_1)/e_2 \tag{24a}$$

$$L(\theta_A) = (\tfrac{1}{2}\frac{e_1^2}{e_2} - e_o) + (k_o - \frac{k_1 e_1}{e_2})v + (\tfrac{1}{2}\frac{k_1^2}{e_2})v^2 \ . \tag{24b}$$

Then, finally, variation with respect to θ_A leads to a quadratic equation for v, with the possibility of two solutions as functions of θ_A. These solutions are considered acceptable only if they give $\Delta << 1$. Considering θ_A as the independent variable, we then have obtained the velocity, width, energy etc., all as functions of θ_A.

We have also made a two parameter Ansatz for XY kinks by taking $\theta_A = \theta_B$, or $\Delta = 0$, in which case we find the static XY kink energy to be $\beta(1-\beta^2/24)$, slightly smaller than the sine-Gordon result. Similarly, a two parameter Ansatz for YZ kinks is made by assuming $\theta_A + \theta_B = \pi$, and we find the static YZ kink energy to be $2\sqrt{\alpha}(1-\beta^2/16)$, which has a stronger field dependence than the sine-Gordon result. These differences are probably due to using xyz components instead of spherical coordinates.

IV. Numerical and Variational Ansatz Results

In Fig. 3 we show results obtained from this Ansatz using $\alpha = 0.04$, as appropriate for TMMC (Regnault et al. 1982), and for a series of fields β ranging from 0.2 to 0.5 (the critical field being $\beta_c = 2\sqrt{\alpha} = 0.4$), and for θ_A ranging from zero to π. For a given value of θ_A,

solving $\frac{\partial L}{\partial \theta_A} = 0$ (using Eq. (24b)) gives two solutions for v, which are then substituted into Eq. (24a) to give Δ, and finally Δ is used in (23b) to obtain the energy. In Fig. 3 we have kept only those solutions which satisfy $|\Delta| < 0.2$. The solid and dashed curves correspond to the two roots for v (plus and minus from the quadratic formula). From the curves of Δ versus θ_A, it is seen that there are two distinct regions which correspond to kinks which are either YZ-like (the approximately linear portions of the curves, near $\theta_A = \frac{1}{2}\pi$) or XY-like (the parabolic segments, generally at $\theta_A \neq \frac{1}{2}\pi$). Note that Δ measures the deviation of the kink from being "flat"; for $\Delta = 0$, we have $\theta_A = \theta_B$, such that both sublattices rotate in the same plane. A nonzero Δ corresponds to a situation in which the two sublattice planes are canted, and in particular, for stable YZ kinks, the canting is toward the field.

In Fig. 3 we also show results of numerical integration of the equations of motion on a discrete lattice. The data points were obtained by using initial profiles from this Ansatz, using both roots for v. We used initial profiles with θ_A over the entire range from zero to π which gave $|\Delta| < 0.2$. Cases where the kink was unstable were obvious -- an unstable YZ kink would deform to an XY kink, accompanied by spin waves. Even for stable kinks, there was usually relaxation accompanied by the emission of spin waves; therefore we have time averaged the kinks in their own (moving) reference frame as a means of removing spin waves from the system. Such time averaging usually produces smooth travelling wave solutions, except in cases where discreteness effects are severe (e.g. for high velocity kinks). The velocity of the resulting profile was measured by taking the center of the kink as the point at which S^y is

zero. We have used lattices ranging from 101 to 301 spins (depending on the kink width), an odd number being necessary to simulate a system with one kink satisfying periodic boundary conditions. Characteristic kink widths can be estimated from Eqs. (6a) and (7) -- typical widths for zero velocity kinks were 10 lattice units (YZ) and 8-40 lattice units (XY). The equations written in terms of xyz components were integrated using a fourth order Adams-Pece predictor corrector method, with a fixed time step of 0.04. Energy conservation and spin length conservation, both to better than 1 part in 10^5, were used as checks of the numerical accuracy.

We have found that only one of the two roots for v always gives stable kink profiles (the dashed curves), the other root can correspond to an unstable branch. The most striking feature of the results, however, is that the stable root corresponds to either an XY or YZ kink, depending on θ_A; the XY and YZ kink branches are continuously connected. Furthermore, for $\frac{1}{4}\beta^2 < \alpha$, where static YZ kinks are unstable, the numerical simulations show that there is a velocity above which YZ kinks are stable, confirming the linear stability analysis results already given.

The energy versus velocity data points from the numerical integration do not agree exactly with the Ansatz calculation, especially for YZ kinks, probably due to discreteness effects for high velocity kinks and also than 5 lattice units) along with the small parameter approximations made to evaluate the Lagrangian ($\sqrt{\alpha}$, β, $\Delta << 1$). For a kink of given energy, the actually velocity is less than that predicted by the Ansatz or sine-Gordon theory, but this effect is most pronounced at higher velocities. We should note that the spin wave velocity in these

units is c = 2, and the greatest discrepancies occur for kink velocities greater than $\cong \frac{1}{2}c$. Also the kink energies may be slightly overestimated by the numerical integration, since it is not always possible to completely eliminate spin waves from the system.

V. Discussion and Conclusions

From Fig. 3, for $\beta \neq \beta_c$, where $\beta_c \equiv 2\sqrt{\alpha}$ the XY branch merges into the YZ branch at some maximum XY velocity less than c. This can be compared to the ferromagnet (J < 0 in (1)), where the critical field is $\beta_c^{Ferro} = \frac{1}{3}\alpha$ (Kumar 1982, Magyari and Thomas, 1982). For $\beta < \beta_c^{Ferro}$, there is also a maximum kink velocity less than c, but the character of the kinks does not change suddenly as one moves along the dispersion curve through the maximum velocity point. There is only a continuously increasing deviation from the sine-Gordon profile.

In the Liebmann et al. Ansatz (1983), as their variational parameter $\frac{1}{2}\theta_m$ (approximately equivalent to θ_A here) increases from zero to $\frac{1}{2}\pi$, the kink geometry ranges from planar to a small amplitude wave packet (i.e. pulse-like). The kink branch resulting from their Ansatz therefore terminates at zero energy and velocity (i.e. no kink). In the Ansatz here, there is no analogous topological decay of the kink as θ_A is varied from zero to $\frac{1}{2}\pi$; the spin profile is always a large amplitude deviation from the ground state configuration, as a result of the boundary conditions. The boundary conditions strongly affect the dynamics.

From our numerical integrations, XY kinks are stable above and below the critical field, for $\alpha = 0.04$, $0.08 < \beta < 0.6$ and $|v/c| < 1$. Even for $\beta > \beta_c$, they show no tendency to decay to lower energy YZ kinks. Whether they can be viewed as slightly perturbed sine-Gordon

kinks is doubtful, especially for $\beta > \beta_c$. For small velocities $v << c$, the two parameter Ansatz reproduces the velocity dependence of the energy as found by Flüggen and Mikeska (1983), with the curvature of E versus v proportional to $(\beta_c^2-\beta^2)^{-1}$. This curvature can be thought of as a kinetic mass for the kink, which diverges and changes sign at the critical field. For fields $\beta < \beta_c$, this mass is positive and the kinks are close to sine-Gordon kinks, but move at speeds less than that predicted by sine-Gordon theory for a given energy. At the critical field, the mass diverges, and there is a continuum of XY kinks with a range of θ_A, all with the same energy and velocity. Magyari and Thomas (1983) have referred to this effect in the corresponding ferromagnet as a "soft velocity change". At the critical field, infinitesimal perturbation of a kink (for instance by varying θ_A) leads to one with the same velocity. Above the critical field, the mass is negative, and the behavior strongly deviates from sine-Gordon. The situation is the same as in the ferromagnet above the critical field, where the kinks are dynamically stable but move in a direction opposite to that predicted by sine-Gordon theory (Wysin et al. 1982). We conclude that XY kinks are not adequately described by sine-Gordon theory, and that there is no structural instability induced at the critical field.

For small velocities $v << c$, the two parameter Ansatz for YZ kinks reproduces the velocity dependence of the energy given by sine-Gordon theory. We find that sine-Gordon theory adequately describes the YZ branch. Concerning stability, we have shown that static YZ kinks are stable only if $\beta > \beta_c$, and that dynamic YZ kinks require a minimum applied field to be stable, where this minimum field decreases with increasing velocity. Stated differently, the only stable YZ kinks have

a velocity greater than some critical velocity which decreases as the field increases. For $\beta < \beta_c$, the critical velocity is positive[+] (see Fig. 3, $\beta = 0.3$); a certain amount of canting of the two sublattice planes toward the field is needed to insure stability. For $\beta = \beta_c$, the critical velocity is zero. For $\beta > \beta_c$, the critical velocity is negative (see Fig. 3, $\beta = 0.5$); a certain amount of canting of these planes away from the field is allowed before instability results. For YZ kinks, stability is determined by the field and the velocity, i.e. there is a stability field (i.e. a minimum field for stability) which depends on velocity.

Finally, we recall that experimental data on TMMC is available for magnetic fields beyond the critical value (e.g. Boucher et al. 1984), and is consistent with a crossover from XY to YZ kinks as suggested here. However, we have found numerically that XY kinks are stable both below and above the critical field. Thus both XY and YZ kinks should carry thermodynamic weight at high fields and be reflected experimentally.

[+]Here positive and negative velocity refer to v as seen in Fig. 3.

References

Boucher, J. P., Regnault, L. P., Rossat-Mignod, J., Renard, J. P., Bouillot, J., Stirling, W. G. and Mezei, F. (1983) Physica 120B, 241.

Boucher, J. P., Regnault, L. P., Pires, A., Rossat-Mignod, J., Henry, Y., Bouillot, J., Stirling, W. G. and Renard J. P. (1984) Workshop on Elementary Excitations and Fluctuations in Magnetic Systems, San Miniato, Italy, to appear in Springer series in Sol. State Sciences.

Boucher, J. P. and Renard, J. P., (1980) Phys. Rev. Lett. 45, 486.

Flüggen, N. and Mikeska, H. J., (1983) Solid St. Comm. 48, 293.

Harada, I., Sasaki, K., Shiba, H., (1981) Solid St. Comm. 40, 29.

Heilmann, I. U., Birgeneau, R. J., Endoh, Y., Reiter, G., Shirane, G., and Holt, S. L., (1979) Solid St. Comm. 31, 607.

Kumar, P., (1982) Phys. Rev. B25, 483.

Liebmann, R., Schöbinger, M., Hackenbracht, D., (1983) J. Phys. C 16, L633.

Magyari, E. and Thomas, H., (1982) Phys. Rev. B25, 531; (1983) J. Phys. C 16, L535.

Mikeska, H. J., (1980) J. Phys. C. 13, 2913.

Regnault, L. P., Boucher, J. P., Rossat-Mignod, J., Renard, J. P., Bouillot, J. and Stirling, W. G., (1982) J. Phys. C. 15, 1261.

Sklyanin, E. K., (1979) Sov. Phys. Dokl. 24, 107.

Wysin, G., Bishop, A. R. and Kumar, P., (1982) J. Phys. C 15, L337; (1984) J. Phys. C 17, 5975.

Wysin, G. M. (1985), Ph.D. Thesis, Cornell University.

Figure Captions

Fig. 1. Geometry for the Ansatz. (a) The dot represents the ground states projected onto the x-axis, the arrow is the spin on the A sublattice at the center of the kink. The dashed line represents the plane in which the tips of the spin vectors $\hat{\sigma}_A$ move in this Ansatz. (b) View of the two ground states as seen looking down the z' axis; the Ansatz assumes that the spins $\hat{\sigma}_A$ move in the circular path connecting them.

Fig. 2. (a) The sum vector $\vec{M}$ as seen in the $x'y'$ coordinate system. ϕ_{sG} rotates through 2π for the kink Ansatz. (b) The difference vector $\vec{N}$ as seen in the $x'y'$ system. The radii of these circles are derived from Fig. 1.

Fig. 3. Kink energy vs. velocity and Δ vs. θ_A for fields (a) $\beta = 0.2$, (b) $\beta = 0.3$, (c) $\beta = 0.4$ (the critical field), (d) $\beta = 0.5$. The solid and dashed curves have been obtained from the two solutions given by the Ansatz. The data points are results of the numerical integration, time averaging initial kink profiles derived from the Ansatz.

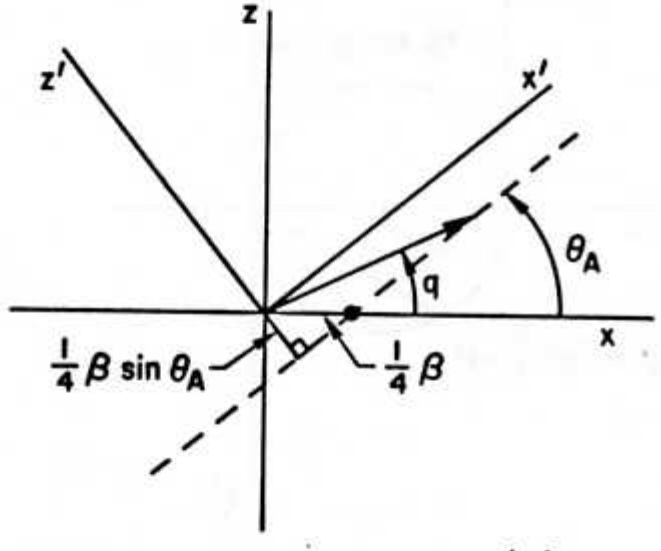
z
z'
x'
θ_A
q
x
$\frac{1}{4}\beta \sin\theta_A$
$\frac{1}{4}\beta$

(a)

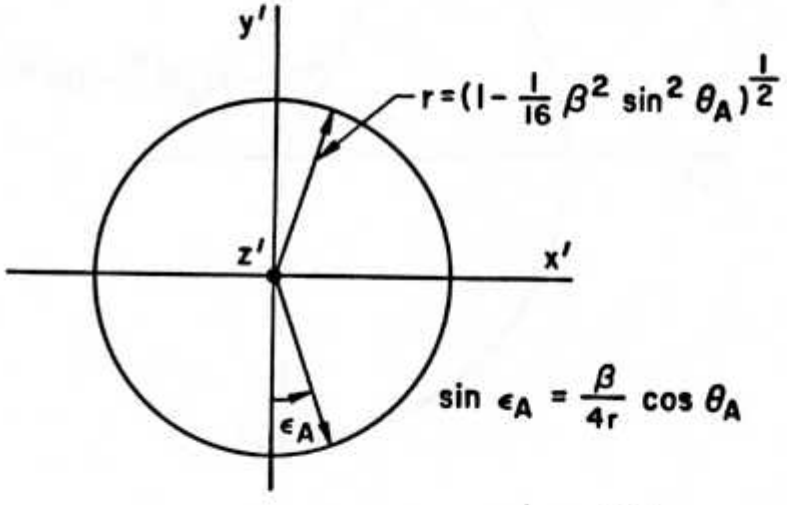
y'
$r=(1-\frac{1}{16}\beta^2 \sin^2\theta_A)^{\frac{1}{2}}$
z'
x'
ϵ_A
$\sin\epsilon_A = \frac{\beta}{4r}\cos\theta_A$

(b)

FIGURE 1.

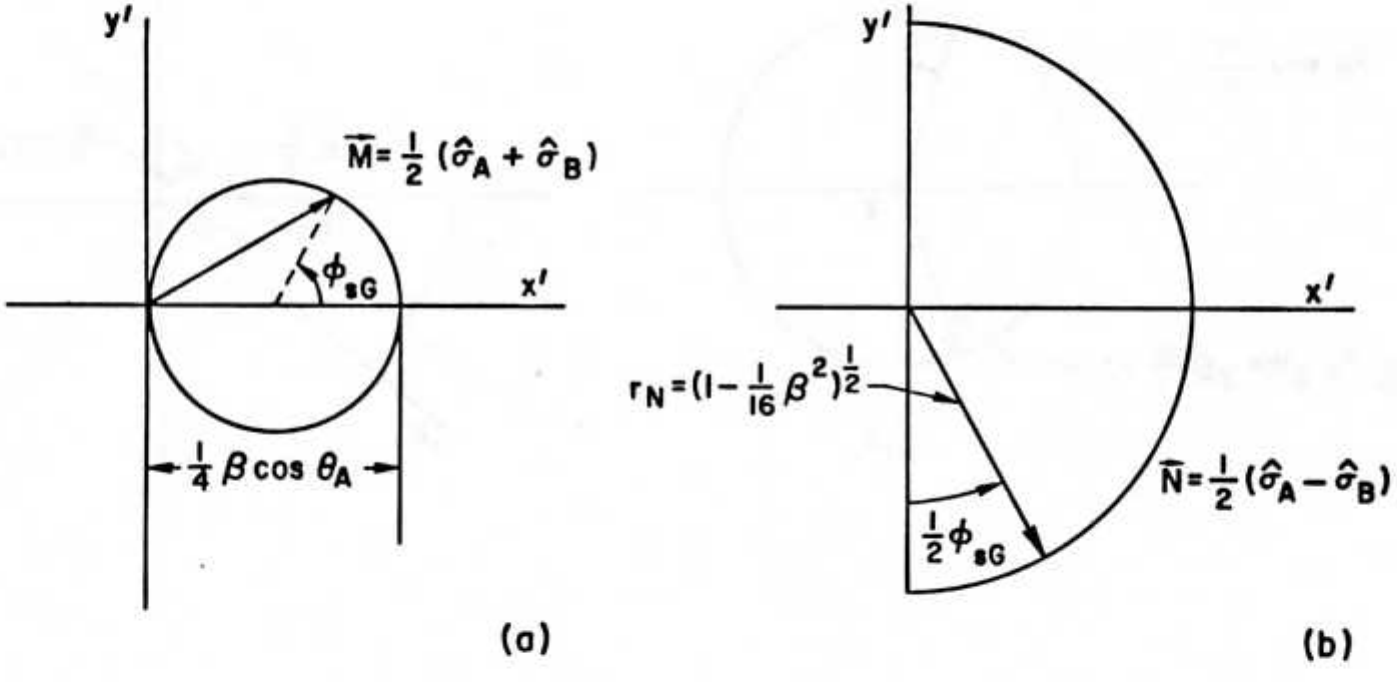
y'
x'
$\bar{M} = \frac{1}{2}(\hat{\sigma}_A + \hat{\sigma}_B)$
ϕ_{sG}
$\frac{1}{4}\beta \cos\theta_A$
(a)
y'
x'
$r_N = (1 - \frac{1}{16}\beta^2)^{\frac{1}{2}}$
$\bar{N} = \frac{1}{2}(\hat{\sigma}_A - \hat{\sigma}_B)$
$\frac{1}{2}\phi_{sG}$
(b)

FIGURE 2.

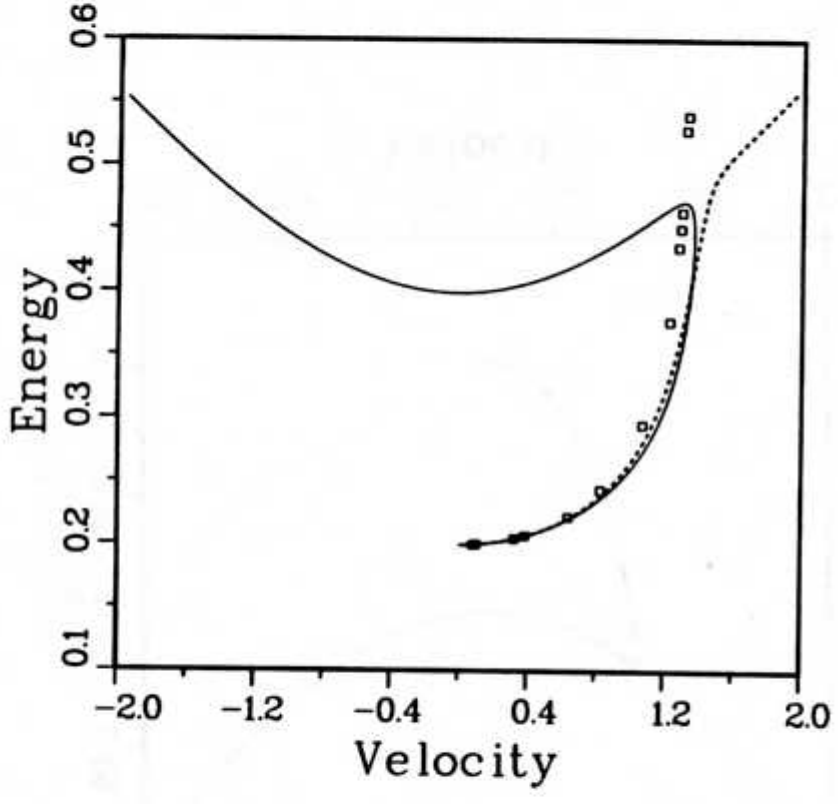
Energy
0.6
0.5
0.4
0.3
0.2
0.1
−2.0
−1.2
−0.4
0.4
1.2
2.0
Velocity

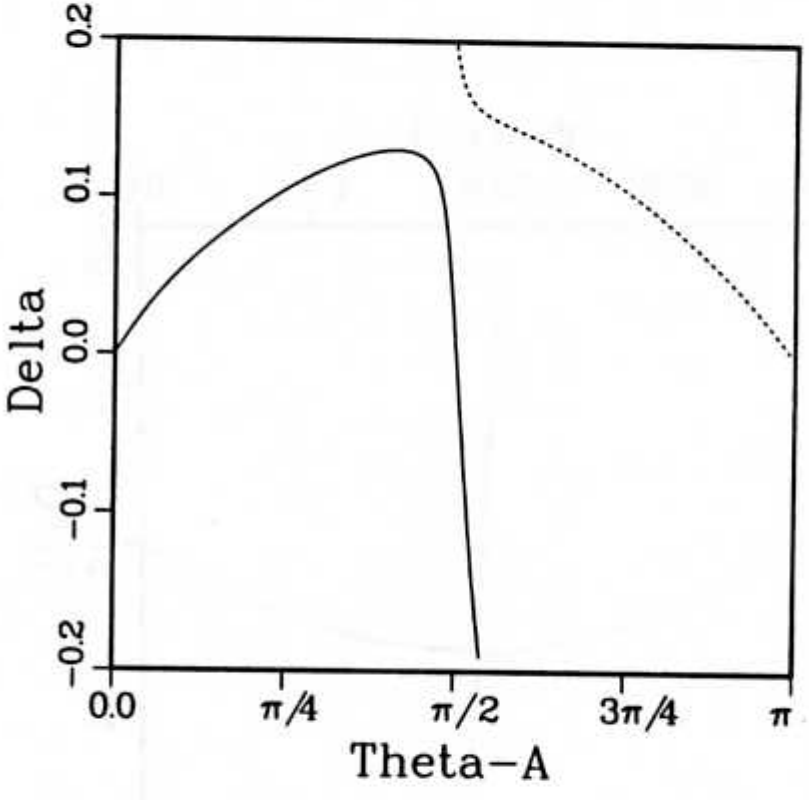
Delta
0.2
0.1
0.0
−0.1
−0.2
0.0
π/4
π/2
3π/4
π
Theta−A

Fig. 3a

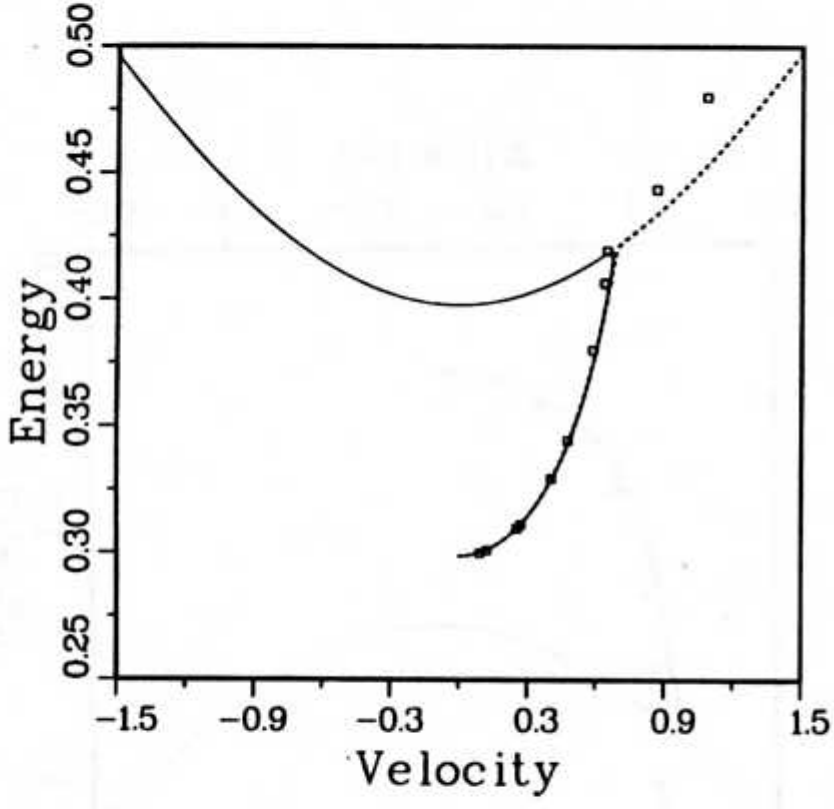
Energy
0.50
0.45
0.40
0.35
0.30
0.25
−1.5
−0.9
−0.3
0.3
0.9
1.5
Velocity

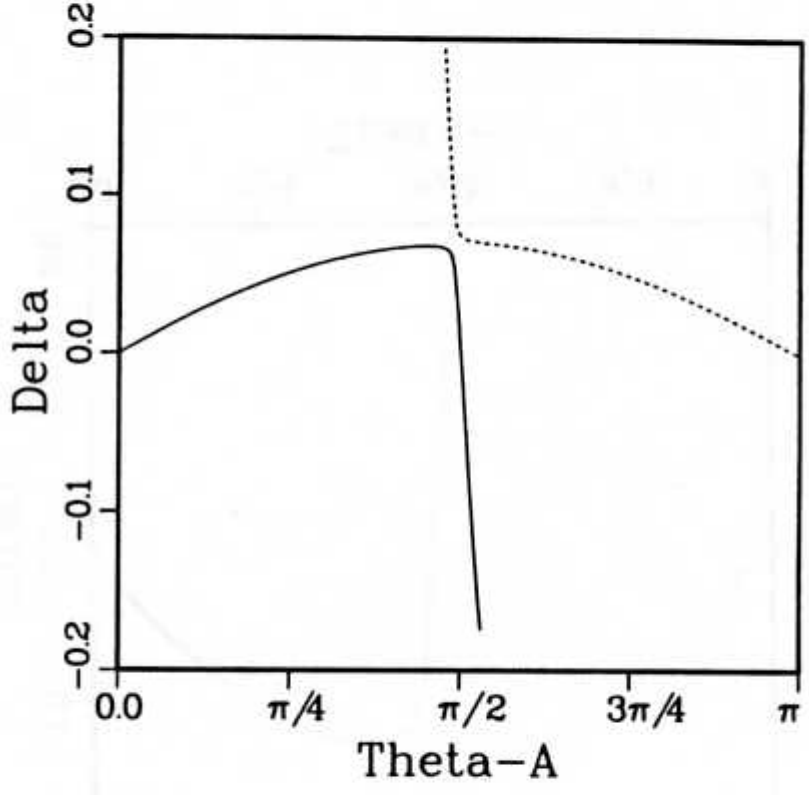
Delta
0.2
0.1
0.0
−0.1
−0.2
0.0
π/4
π/2
3π/4
π
Theta−A

Fig. 2b

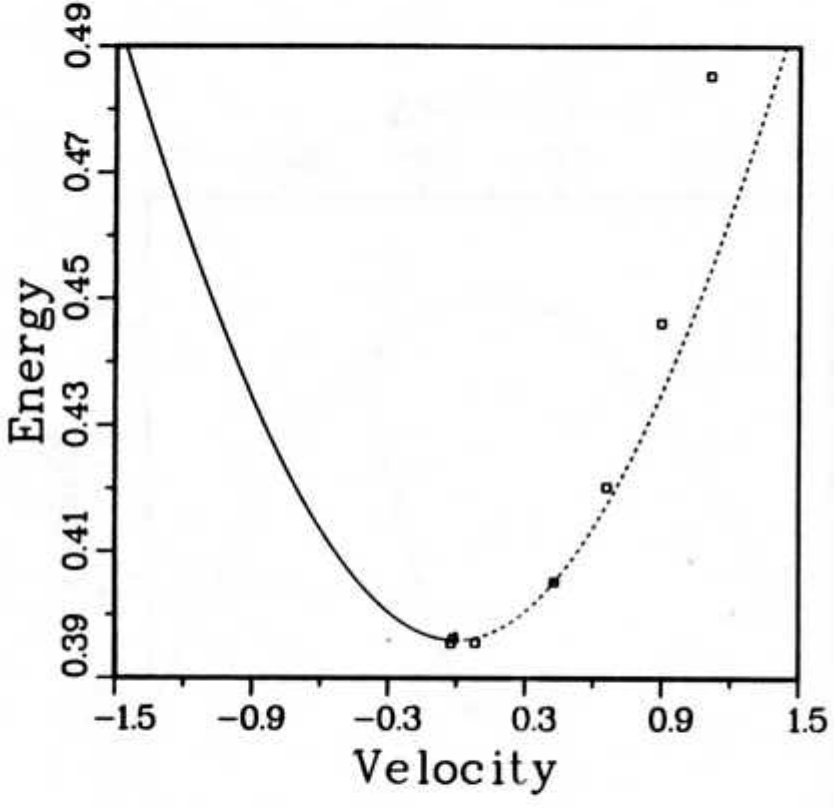
Energy
0.49
0.47
0.45
0.43
0.41
0.39
−1.5
−0.9
−0.3
0.3
0.9
1.5
Velocity

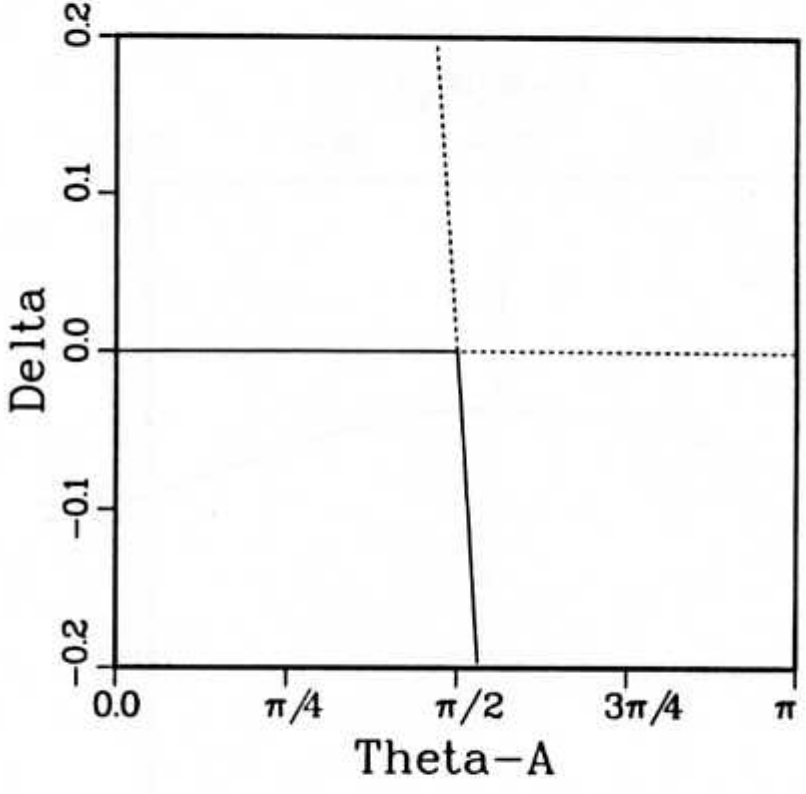
Delta
0.2
0.1
0.0
−0.1
−0.2
0.0
π/4
π/2
3π/4
π
Theta−A

Fig. 3c

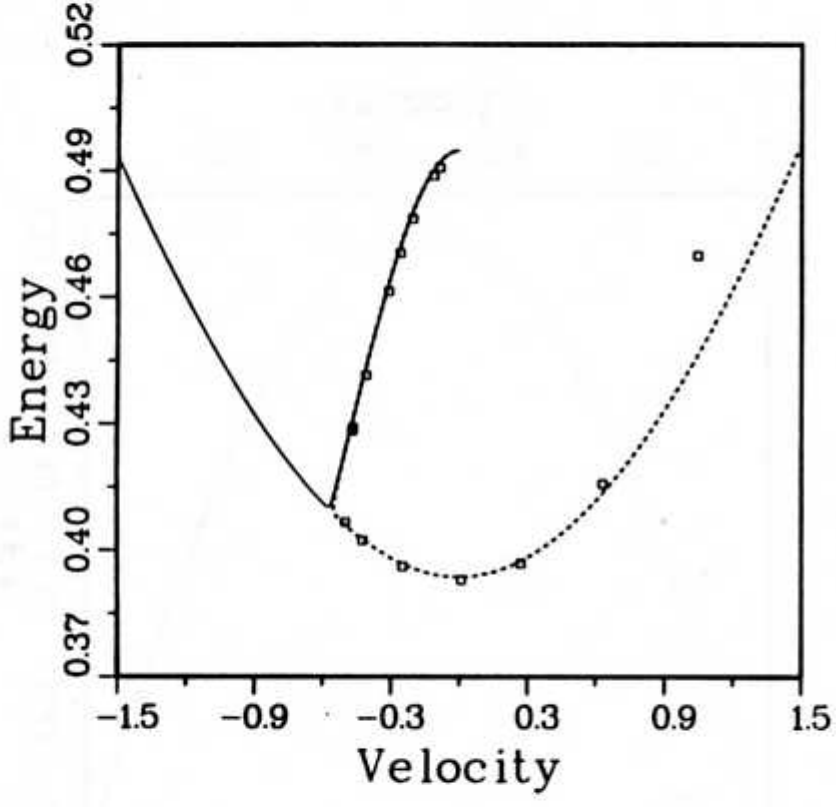
Energy
0.52
0.49
0.46
0.43
0.40
0.37
−1.5
−0.9
−0.3
0.3
0.9
1.5
Velocity

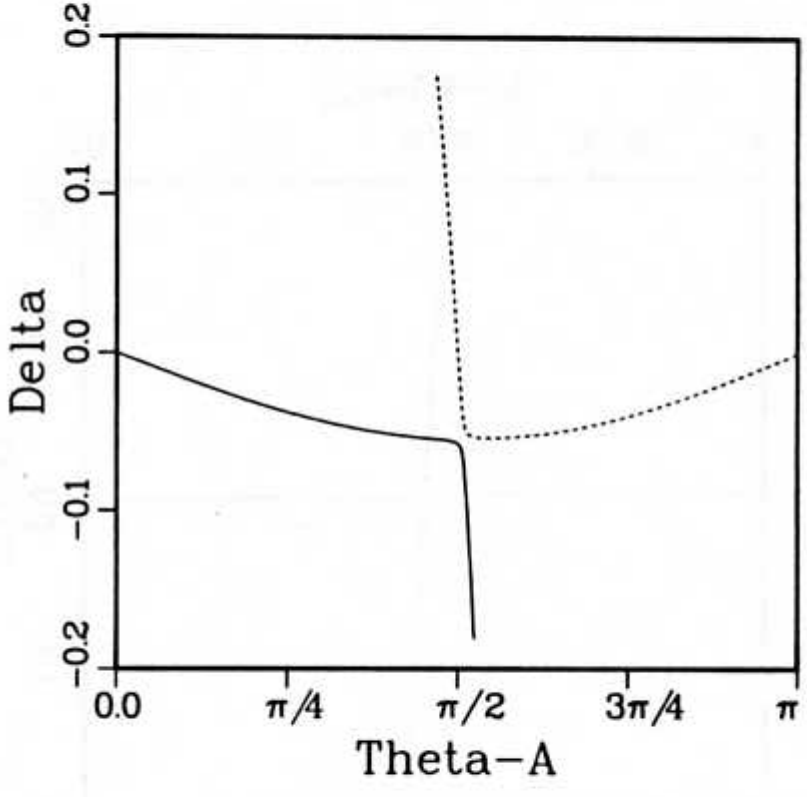
Delta
0.2
0.1
0.0
−0.1
−0.2
0.0
π/4
π/2
3π/4
π
Theta−A

Fig. 3d